The Examination of Afyonkarahisar's Geothermal System Corrosion

A. Buyuksagis & S. Erol

Journal of Materials Engineering and Performance

ISSN 1059-9495
Volume 22
Number 2

J. of Materi Eng and Perform (2013)
22:563-573
DOI 10.1007/s11665-012-0252-x

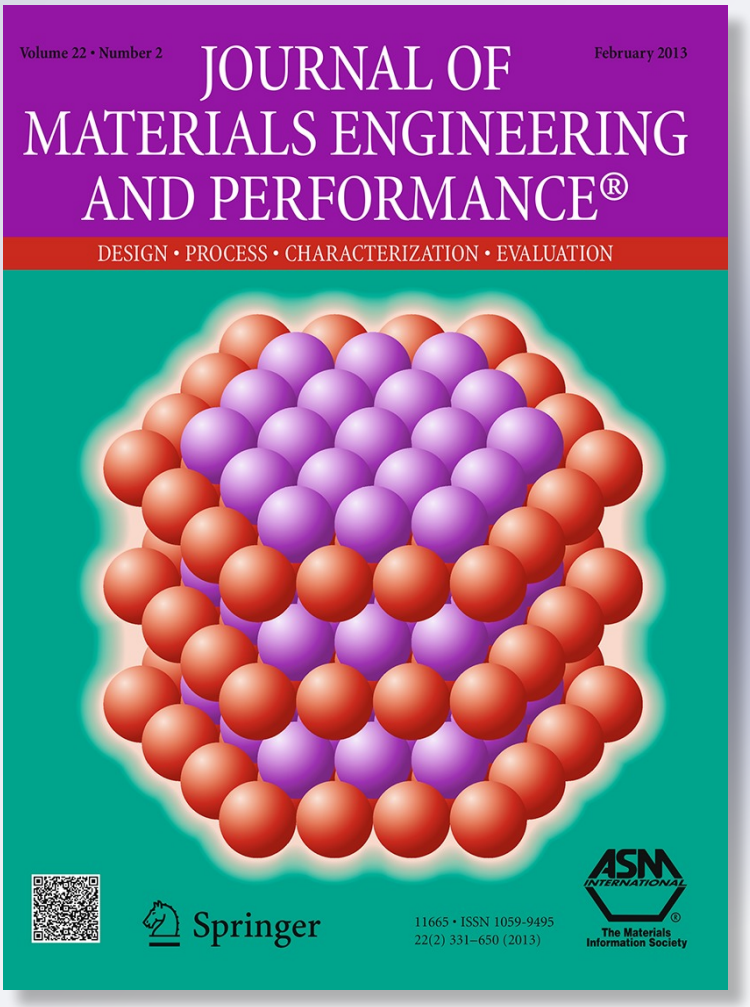

Springer

JMEPEG (2013) 22:563–573
DOI: 10.1007/s11665-012-0252-x

1059-9495/$19.00

The Examination of Afyonkarahisar's Geothermal System Corrosion

A. Buyuksagis and S. Erol

(Submitted August 2, 2010; in revised form October 6, 2011; published online May 26, 2012)

Corrosion and scaling of metal surfaces are the major problems caused by geothermal fluids when metallic structures are used. This article describes a study of corrosion and scaling problems in the Afyonkarahisar Geothermal Heating System (AFJET) in Afyonkarahisar, Turkey. Water analysis, XRD, SEM, EDX, IC, ICP-OES analyses, and electrochemical methods were used in this study. Pentasodium triphosphate ($Na_5P_3O_{10}$), maleic anhydride ($C_4H_2O_3$), and 1,3-benzendisulfonic acid disodium salt ($C_6H_4Na_2O_6S_2$) were used as corrosion inhibitors. Tests were carried out using geothermal water from AF11 well. The experimental temperatures were chosen as 298, 333, and 358 K. Inhibitor concentrations were chosen as 1×10^{-1}, 1×10^{-2}, 1×10^{-3}, and 1×10^{-4} mol/dm^3. Moreover, mixed inhibitor solutions were prepared using the inhibitor concentrations that showed the best inhibition. The first mixed inhibitor solution showed 96% inhibition. The second mixed inhibitor solution showed 90% inhibition. The tested inhibitors act as anodic inhibitors. XRD analysis shows that there is $CaCO_3$ aragonite scaling in the system. Increasing TDS, alkalinity, and hardness all promote scale formation. The photomicrographs from SEM-EDX and the metallographic microscope show that the tested inhibitors form a protective film on the surface. IC and ICP-OES analyses show that the concentration of Ca^{2+} is very high, which supports scale formation.

Keywords corrosion, geothermal fluid, inhibitor, scale, XRD

1. Introduction

Corrosion of metal surfaces and scale formation are among the important problems in systems using geothermal fluid (Ref 1, 2). The mechanism and kinetics of corrosion depend on the physical and chemical characteristics of the environment as well as on the construction material. All forms of corrosion can occur in geothermal equipment, making it hard to predict the specific form in each case. The chemical species in geothermal fluids that determine the corrosion of metals are mainly oxygen, hydrogen ions, chloride ions, hydrogen sulfide, carbon dioxide, and ammonia (Ref 3, 4). A number of methods have been tested to control corrosion and scaling in geothermal systems. Common among these are the use of inhibitors, controlling the carbonate-bicarbonate equilibrium by controlling the pH and CO_2 partial pressure, and periodic cleaning (Ref 4-6). The utilization of scale inhibitors is the most common and promising method of combating scaling problems in geothermal operations. The main problem is to select the most suitable inhibitor among the hundreds of different chemicals on the market (Ref 7, 8).

Research related to scale formation and corrosion in geothermal systems have continued. Related to this Xyla et al. (Ref 9) examined the effect of four synthetically prepared compounds on the spontaneous precipitation of calcium carbonate ($CaCO_3$) in aqueous media. The existence of the P-C-C-P bonds in molecules of the organophosphorus compounds resulted in the most effective inhibitors. Gallup (Ref 10) explored the inhibition of ferric silicate scales from high temperature, hyper saline geothermal brines. Scale control was achieved by injecting sufficient reducing agent into the brine to reduce Fe^{3+} to Fe^{2+}. Batis et al. (Ref 7) examined the corrosion behavior of steel in a solution simulating geothermal fluid from the Sousaki field in Greece. Gallup (Ref 11) added silicate complexing/sequestering agents into geothermal brines to achieve metal-silicate scale inhibition. The results show that complexing/sequestering agents may be economically advantageous, and easier and safer to use under certain circumstances.

Morizot and Neville (Ref 12) studied the effect of polycarboxylic acid (PAA) and used an electrochemical technique to assess the extent of film formation. The presence of calcium and magnesium ions in the solution and the cathodic electrochemical activity at the metal surface have been to enhance the inhibitor film formation by promoting the transport of the inhibitor from the solution to the metal surface. Gallup and Barcelon (Ref 13) acid precursors appear to be acceptable alternatives to strong acids as a means of limiting corrosion transport. In their study, Richter et al. (Ref 14) examined an Icelandic geothermal district heating system. The method of differential electric resistance measurement, which is not electrochemical, gave the best result. Banas et al. (Ref 15) examined the corrosion behavior of st 37 steel in an H_2O-CO_2-H_2S system. The results showed that CO_2 and H_2S affected the stability of the passive film under the chosen temperature and high pressure.

This article reports research on ways of preventing corrosion in the Afyonkarahisar Geothermal Heating System (AFJET). Water analysis, x-ray diffraction (XRD), scanning electron microscopy (SEM), energy dispersive x-ray spectroscopy (EDX), ion chromatography (IC), inductively coupled plasma

A. Buyuksagis and **S. Erol**, Science and Art Faculty, Afyon Kocatepe University, Afyon, Turkey. Contact e-mail: absagis@aku.edu.tr.

optical emission spectrometry (ICP-OES) analyses, and electrochemical methods were used in this study. Pentasodium triphosphate ($Na_5P_3O_{10}$), maleic anhydride ($C_4H_2O_3$), and 1,3-benzendisulfonic acid disodium salt ($C_6H_4Na_2O_6S_2$) were used as corrosion. The experimental temperatures were chosen as 298, 333, and 358 K. Inhibitor concentrations were chosen as 1×10^{-1}, 1×10^{-2}, 1×10^{-3}, and 1×10^{-4} mol/dm^3. Moreover, mixed inhibitor solutions were prepared using the concentrations that showed the best inhibition.

2. Materials and Methods

2.1 Corrosion Experiments

A standard one-compartment three-electrode cell was used. The reference electrode was Hg/Hg_2Cl_2 (sat., KCl) and the counter electrode was a platinum sheet. In this study, all electrode potential values were referred to this reference electrode. The working electrode was a st 37 steel (DIN 17100 or AISI 1018) sample of 1.96×10^{-5} m^2 in electrode area embedded in polyester. The chemical composition of the working electrode is shown in Table 1 (wt.%).

Before each experiment, the electrode was polished with 1200 grit emery paper, washed thoroughly with bi-distilled water, then transferred to the cell. In all cases, the electrode was immersed for 1800 s in the cell before measurements began. During each experiment, solutions were mixed with a magnetic stirrer.

Measurements were obtained using a system consisting of a Wenking PGS 2000D potentiostat and a Pentium IV computer. To determine the corrosion rates, the anodic and cathodic Tafel regions extrapolating to corrosion potentials were used. Tests were always repeated at least three times. Corrosion characteristics are identified by corrosion potential (E_{cor}), cathodic Tafel slope (β_c), anodic Tafel slope (β_a), corrosion rate (i_{cor}), % surface coated fraction, and inhibition percentage. Surface coated fraction and inhibition percentage values were calculated from the formulae below:

$$\text{surface coated fraction} = \frac{i_0 - i_c}{i_0} \quad \text{(Eq 1)}$$

$$\text{Inhibition}\% = \frac{i_0 - i_c}{i_0} \times 100 \quad \text{(Eq 2)}$$

where i_c and i_0 represent corrosion currents with and without inhibitor, respectively. Current-potential curves were obtained by the potentiodynamic method at a scanning rate of 2 mV/s.

2.2 Water Analyses

A sample of water from the geothermal reservoir was taken from well AF11 in order to examine corrosion phenomena. All experiments were carried out in this AF11 well fluid, designated below simply as AF11. Inhibitors at concentrations of 1×10^{-1}, 1×10^{-2}, 1×10^{-3}, and 1×10^{-4} mol/dm^3 were added into the AF11 well fluid. pH and potential values of the samples were measured using a WTW pH 330i/SET pH meter, and conductivity and total dissolved solids (TDS) values were measured with a WTW con 330i/SET conductometer. Total hardness experiments are performed according to TS 266 (Ref 16). According to this, 10 cm^3 geothermal fluid is taken to Erlenmeyer flask and then 0.2 cm^3 NH_3/NH_4^+ tampon solution and very little eriochromo black T indicator taken with spatula tip are added into it. And then it is titrated with 0.01 mol/dm^3 ethylene diamine tetra acetic acid (EDTA-$C_{10}H_{16}N_2O_8$) solution until the color turns from wine red to blue. Total hardness is formulated as follows:

$$\text{total hardness (FSD)} = \frac{V_{\text{EDTA}}(\text{cm}^3) \times M_{\text{EDTA}}(\text{mol/dm}^3) \times MA_{\text{CaCO}_3}(\text{g/mol})}{V_{\text{sample}}(\text{cm}^3) \times 10} \times 1000, \quad \text{(Eq 3)}$$

where V_{EDTA} is the Spending 0.01 mol/dm^3 EDTA solution; M_{EDTA} is the 0.01 mol/dm^3 EDTA solution concentration; MA_{CaCO_3} is the $CaCO_3$'s mole mass; and V_{sample} is the Geothermal fluid volume as cm^3.

In this study, ion chromatography (IC-Dionex; GP50) and inductively coupled plasma optical emission spectroscopy (ICP-OES; ICP-AES Varian Liberty Series2 EL97093438) analyses were carried out on the geothermal fluid samples.

2.3 XRD Analysis

Scale sample inner side of the pipe (formed in natural conditions) was analyzed by XRD. Scale sample was obtained from the geothermal installation out of collection pond mouth. Scale sample was pulverized in a mortar, passed through a 100 mesh sieve and then analyzed using a Shimadzu XRD-6000 instrument.

2.4 SEM-EDX and Metal Microscopy Analyses

SEM and EDX analyses were obtained using a LEO 1430 VP scanning electron microscope. Metal microscopy analyses were obtained using an OLYMPUS BX60 metallographic microscope. Prior to examination, the surface of the st 37 steel was prepared by standard metallographic methods. The steel was first ground using progressively finer grades of emery paper (240, 400, 600, 800, 1000, and 1200 grit paper) in a Metkon Gripo 2V Grinder Polisher (250-300 rpm). Samples were washed using bi-distilled water and then alcohol. Samples were dried in a current of warm air. St 37 steel samples were immersed in geothermal water for 2 and 9 days (at 298 K) without inhibitor and with first mixed inhibitor solution. Surface photomicrographs were taken from SEM and the metallographic microscope. EDX analyses were also made on these samples.

Table 1 Chemical composition (wt.%) of the st 37 steel

	C	Mn	Si	P	S	Cr	Ni	Mo
st 37	0.10	0.40	0.25	0.45	0.45	…	…	…

3. Experimental Results and Discussions

3.1 The Results of Corrosion Experiments

Corrosion parameters that were obtained in AF11 and AF11 + x mol/dm^3 inhibitor solutions at 358 K are shown in Table 2. The current potential curves for each inhibitor are shown in Fig. 1.

As shown in Table 2 (Fig 1), $C_4H_2O_3$ gave 68% inhibition at 1×10^{-2} and 1×10^{-4} mol/dm^3 concentrations and 82% inhibition at a concentration of 1×10^{-3} mol/dm^3. $C_6H_4Na_2O_6S_2$ showed 90% inhibition at concentrations of 1×10^{-2} mol/dm^3 and 82% inhibition at concentrations of 1×10^{-3} mol/dm^3. These results can be explained on the basis that the form of benzene disulfonic acid disodium salt is a benzene ring and has a double bond. The efficiency of the inhibitor increases by functional groups and chemical bonds (Ref 17, 18). $Na_5P_3O_{10}$ inhibitor showed 68% inhibition in 1×10^{-2} and 1×10^{-3} mol/dm^3 concentrations.

The inhibitors showed the best inhibition at concentrations of 1×10^{-3} mol/dm^3. Current-potential curves obtained in AF11 + 1×10^{-3} mol/dm^3 inhibitor solutions (333 K) are shown in Fig. 2(a). Mixed inhibitor solutions were prepared using the concentrations that showed the best inhibition. Current potential curves AF11 + x mol/dm^3 mixed inhibitor solutions at 333 K are shown in Fig. 2(b).

The corrosion characteristics in 10^{-3} mol/dm^3 inhibitor concentrations at 333 and 298 K are shown in Table 3.

As shown in Table 3, $C_4H_2O_3$ gave 68% inhibition at a concentration of 1×10^{-3} mol/dm^3 at 298 K and 44% inhibition at a concentration of 1×10^{-3} mol/dm^3 at 333 K (Fig. 2a). $C_6H_4Na_2O_6S_2$ showed 21% inhibition at concentrations of 1×10^{-3} mol/dm^3 at 298 K and 44% inhibition at concentrations of 1×10^{-3} mol/dm^3 at 333 K. $Na_5P_3O_{10}$ inhibitor showed 44% inhibition in 1×10^{-3} mol/dm^3 at 298 K and 75% inhibition at concentrations of 1×10^{-3} mol/dm^3 at 333 K.

The corrosion characteristics in AF11 and AF11 + x mol/dm^3 mixed inhibitor solutions at 298 K are shown in Table 4.

Inhibitor mixture solutions are more effective in controlling corrosion. As seen in Table 4 and Fig. 2(b), 96% inhibition is obtained in the first mixture inhibitor solution (AF11 + 1×10 3 mol/dm^3 $C_4H_2O_3$ + 1×10^{-2} mol/dm^3 $C_6H_4Na_2O_6S_2$ + 1×10^{-3} mol/dm^3 $Na_5P_3O_{10}$).

This may be explained by the fact that there are negative and positive charge excesses on oxygen, sulfide, ringed structure, and $Na_5P_3O_{10}$ which exist in inhibitor structures. Phosphates are used to prevent corrosion of iron; the formation of phosphate layer prevents dissolution of metal oxide surface. It stabilizes the passiveness of the surface. Many metals which

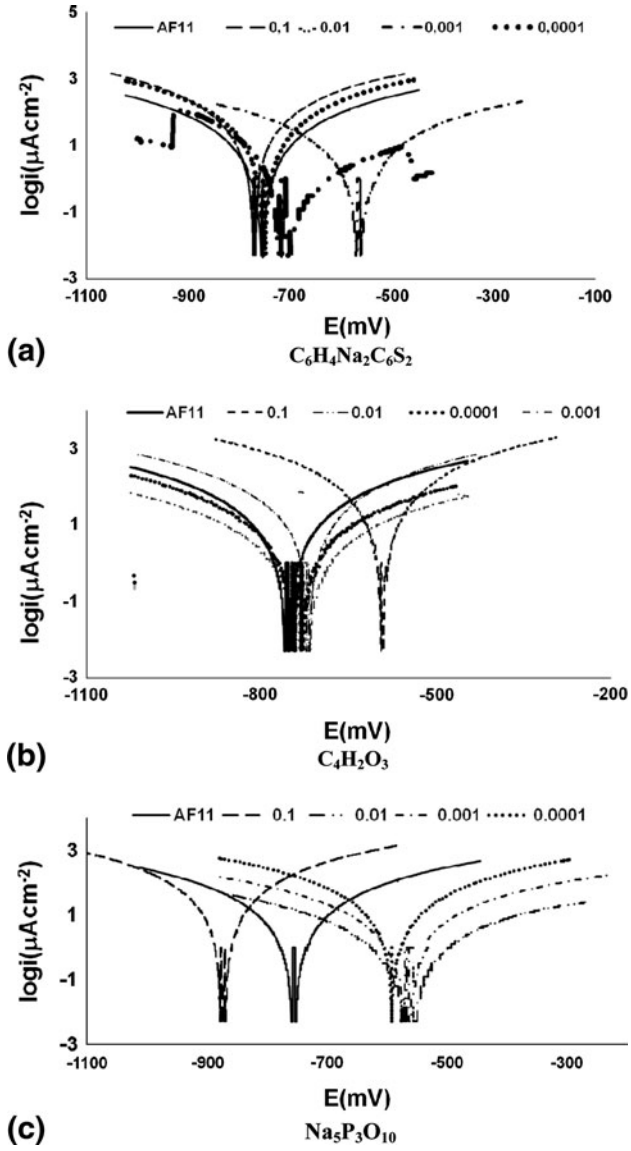

Fig. 1 Current-potential curves obtained in AF11 + x mol/dm^3 inhibitor solutions (at 358 K)

Table 2 Corrosion characteristics obtained in AF11 and AF11 + mol/dm^3 M inhibitor solutions at 358 K

	β_a, mV	$-\beta_c$, mV	$-E_{cor}$, mV	i_{cor}, μA/cm^2	% inhibition, η	Surface coated fraction, θ
AF11	200	222	735	17.78	…	…
+1×10^{-1} mol/dm^3 $C_4H_2O_3$	200	200	875	56.23	…	…
+1×10^{-2} mol/dm^3 $C_4H_2O_3$	200	200	720	5.62	68	0.68
+1×10^{-3} mol/dm^3 $C_4H_2O_3$	100	100	610	3.16	82	0.82
+ 1×10^{-4} mol/dm^3 $C_4H_2O_3$	400	670	725	5.62	68	0.68
+1×10^{-1} mol/dm^3 $C_6H_4Na_2O_6S_2$	166	156	760	56.23	…	…
+1×10^{-2} mol/dm^3 $C_6H_4Na_2O_6S_2$	333	154	710	1.78	90	0.90
+1×10^{-3} mol/dm^3 $C_6H_4Na_2O_6S_2$	200	180	560	3.16	82	0.82
+1×10^{-4} mol/dm^3 $C_6H_4Na_2O_6S_2$	200	200	735	31.6	…	…
+1×10^{-1} mol/dm^3 $Na_5P_3O_{10}$	200	200	875	56.23	…	…
+1×10^{-2} mol/dm^3 $Na_5P_3O_{10}$	125	166	620	5.62	68	0.68
+1×10^{-3} mol/dm^3 $Na_5P_3O_{10}$	100	200	600	5.62	68	0.68
+1×10^{-4} mol/dm^3 $Na_5P_3O_{10}$	250	166	590	31.6	…	…

… no inhibition

are important technically are transition metals that have electron spaces in electron circles. There are ionic or covalent bonds between the metal surface atoms and with inhibitor anions according to the type of the anion. The characteristics of the bonds determine the efficiency of the inhibitor. When inhibitors are absorbed on the surface of metal, they form an energy conservation with metal atoms and chemical bonds. The formed energy barrier difficulties the transition metal ions to solution or reduces corrosion by effecting cathodic reaction. The organic molecular must be absorbed in the metal surface to indicate the features of the inhibitor. There will be a load distribution with the absorption of the inhibitor on the metal surface and this will have a specific potential for the ionic double layer. The capacitance of double layer formed on metal surface can be ±. The effects of the functional groups in organic molecular increase the efficiency of the inhibitors. When functional groups, double bonds and three bonds, electrons in organic molecular can interact with the metal and change zero load potential and provide inhibition (Ref 17, 18). 90% inhibition is obtained in the second mixture inhibitor solution (AF11 + 1×10^{-2} mol/dm^3 $C_6H_4Na_2O_6S_2$ + 1×10^{-3} mol/dm^3 $Na_5P_3O_{10}$). E_{cor} values shift to more positive potentials in AF11 + x mol/dm^3 inhibitor solutions compared to AF11's E_{cor} values. This shows that inhibitors are effective at positive potentials; they act as anodic inhibitors.

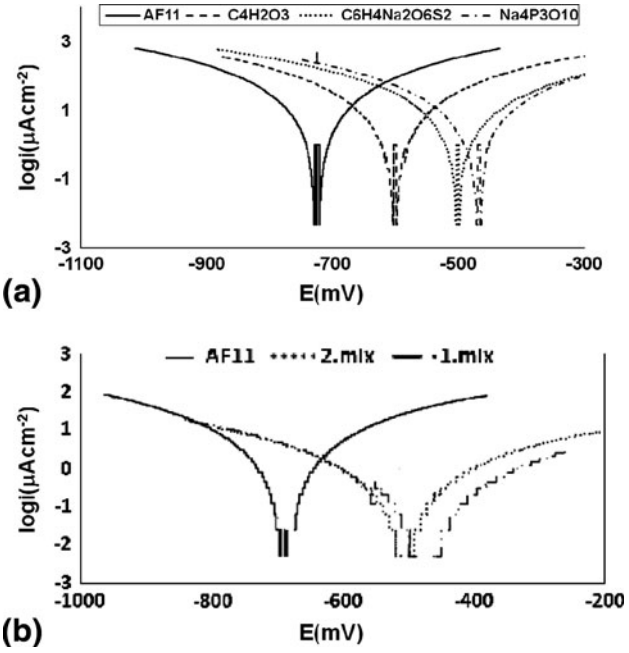

Fig. 2 (a) Current-potential curves obtained in AF11 + 1×10 3 mol/dm^3 inhibitor solutions (333 K). (b) Current-potential curves performed in AF11 and AF11 + mixed inhibitor solutions 333 K (first mixture: AF11 + 1×10^{-3} mol/dm^3 $C_4H_2O_3$ + 1×10^{-2} mol/dm^3 $C_6H_4Na_2O_6S_2$ + 1×10^{-3} mol/dm^3 $Na_5P_3O_{10}$, second mixture: AF11 + 1×10^{-2} mol/dm^3 $C_6H_4Na_2O_6S_2$ + 1×10^{-3} mol/dm^3 $Na_5P_3O_{10}$)

3.2 The Results of Water Analyses

The measured pH, potential, conductivity, TDS, salinity, and total hardness values of AF11 and AF11 + x mol/dm^3 inhibitors solutions are shown in Table 5.

These inhibitors are effective in preventing corrosion when the pH exceeds 8 (Table 5) in AF11 + x mol/dm^3 inhibitor solutions. If TDS is between 750 and 1050 mg/dm^3 has better inhibition. AF11's total hardness is 44 French hardness (FSD). If total hardness is under 44 FSD after adding inhibitors into AF11, the inhibitor is effective in preventing corrosion. If the salinity range is between 0.7 and 0.9 parts per thousand (ppt) inhibitors are effective.

Table 3 The corrosion characteristics obtained for 298 K and 333 K in AF11 and AF11 + 1×10^{-3} mol/dm^3 inhibitor solutions

T, K		β_a, mV	$-\beta_c$, mV	$-E_{cor}$, mV	i_{cor}, μA/cm^2	% inhibition, η	Surface coated fraction, θ
298 K	AF11	100	400	585	10	…	…
	+1×10^{-3} mol/dm^3 $C_4H_2O_3$	100	100	600	3.16	68	0.68
	+1×10^{-3} mol/dm^3 $C_6H_4Na_2O_6S_2$	110	120	620	7.94	21	0.21
	+1×10^{-3} mol/dm^3 $Na_5P_3O_{10}$	100	200	600	5.62	44	0.44
333 K	AF11	500	625	720	31.6	…	…
	+ 1×10^{-3} mol/dm^3 $C_4H_2O_3$	250	250	585	17.78	44	0.44
	+1×10^{-3} mol/dm^3 $C_6H_4Na_2O_6S_2$	200	250	495	17.78	44	0.44
	+1×10^{-3} mol/dm^3 $Na_5P_3O_{10}$	125	166	490	7.94	75	0.75

Table 4 The corrosion characteristics in AF11 and AF11 +x mol/dm^3 mixed inhibitor solutions at 298 K

	β_a, mV	$-\beta_c$, mV	$-E_{cor}$, mV	i_{cor}, μA/cm^2	% inhibition, η	Surface coated fraction, θ
AF11	100	400	585	10		…
+1 mixed inhibitors	222	200	535	0.4	96	0.96
+2 mixed inhibitors	277	250	540	1.0	90	0.90

First mixed inhibitors: 1×10^{-3} mol/dm^3 $C_4H_2O_3$ + 1×10^{-2} mol/dm^3 $C_6H_4Na_2O_6S_2$ + 1×10^{-3} mol/dm^3 $Na_5P_3O_{10}$. Second mixed inhibitors: 1×10^{-2} mol/dm^3 $C_6H_4Na_2O_6S_2$ + 1×10^{-3} mol/dm^3 $Na_5P_3O_{10}$

Table 5 pH, potential, TDS, salinity, conductivity, and total hardness values measured in AF11 and AF11 + x mol/dm^3 inhibitors solutions

	pH	−*U*, mV	TDS, mg/dm^3	Salinity, ppt	Conductivity, mS/cm	Total hardness FSD, mg/dm^3
AF11	7.6	58.9	820	0.7	1615	44
$+1 \times 10^{-1}$ mol/dm^3 $C_4H_2O_3$	2.2	268.2	10200	3.5	5860	70
$+1 \times 10^{-2}$ mol/dm^3 $C_4H_2O_3$	2.3	259.3	1020	1.0	2090	90
$+1 \times 10^{-3}$ mol/dm^3 $C_4H_2O_3$	8.7	121.1	756	0.7	1536	40
$++ 1 \times 10^{-4}$ mol/dm^3 $C_4H_2O_3$	2.5	253.6	980	0.9	1983	70
$+1 \times 10^{-1}$ mol/dm^3 $C_6H_4Na_2O_6S_2$	7.5	53.9	1998	2.3	4300	70
$+1 \times 10^{-2}$ mol/dm^3 $C_6H_4Na_2O_6S_2$	8.2	93.6	910	0.9	1848	40
$+1 \times 10^{-3}$ mol/dm^3 $C_6H_4Na_2O_6S_2$	8.6	116.8	778	0.7	1572	36
$+1 \times 10^{-4}$ mol/dm^3 $C_6H_4Na_2O_6S_2$	7.3	51.5	767	0.7	1552	70
$+1 \times 10^{-1}$ mol/dm^3 $Na_5P_3O_{10}$	8.5	113.5	9200	2.3	4100	70
$+1 \times 10^{-2}$ mol/dm^3 $Na_5P_3O_{10}$	8.1	99.8	920	0.9	1840	35
$+1 \times 10^{-3}$ mol/dm^3 $Na_5P_3O_{10}$	8.2	94.0	764	0.7	1543	30
$+1 \times 10^{-4}$ mol/dm^3 $Na_5P_3O_{10}$	7.6	56.7	763	0.7	1537	60

pH is an important characteristic in geothermal well fluids. If steel is exposed to geothermal fluids having pH 6.5 and high CO_2 (for example, mg/dm^3), there will be hydrogen evolution and acidic corrosion. In weaker acids (e.g., acetic or carbonic) dissolution of the oxide occurs at a higher pH, hence the corrosion rate of iron increases accompanied by hydrogen evolution at pH 5 or 6. In other words, at a low pH value there is more available of H^+ react with the metal and dissolve the barrier oxide films using a strong acid, compared to a weak acid (Ref 19-25). The increased corrosion rate of iron as pH decreases is not caused alone by hydrogen evolution in fact, greater accessibility of oxygen to the metal surface on dissolution of the surface oxide favors oxygen depolarization which is often the more important reason (Ref 26). There will be localized pitting instead of general corrosion in geothermal fluids having pH 8. This is aggravated if there is dissolved oxygen in the geothermal fluid. Pitting corrosion is localized attack, the rate of corrosion being greater at some areas than the others. If appreciable attack is confined to a relatively small fixed area of metal, acting as anode, the resultant pits are described as deep. If the area of attack is relatively larger and not so deep, these pits are called shallow. Many metals when subjected to high velocity liquids undergo a pitting type of corrosion called impingement attack or sometimes corrosion erosion (Ref 27). Geothermal fluids contain dissolved calcium and magnesium salts in varying concentrations, depending on the source and location of the water. If the concentration of such salts is high, the water is called hard; otherwise it is soft. The mechanism of protection afforded by a hard water is the natural deposition of a thin diffusion-barrier film, composed largely of $CaCO_3$, on the metal surface. This film retards diffusion of dissolved oxygen to cathodic areas, supplementing the natural corrosion barrier of $Fe(OH)_2$. However, hardness alone is not the only factor that determines whether a protective film is possible. Ability of $CaCO_3$ to precipitate on the metal surface also depends on total acidity or alkalinity, pH, and concentration of dissolved solids in the water. The well components form a scale as a result of carbonate deposition in such geothermal fluids. It is possible to obtain information about the corrosive potential of water or its protective power on an iron surface. The pH and redox potential diagram is called a Pourbaix diagram (Ref 28-31). It can accurately predict the nature of the corrosion products that would be thermodynamically stable on the steel surface, provided enough time is allowed for the system to reach an equilibrium state.

If corrosion rate increases, inhibition can decrease. In acidic media, corrosion rate is greater than the alkaline media. As the metal surface is not coated with hydroxides and oxides in acidic medium. Although potential values measured by using a conductometer are in the cathodic region, E_{cor} values shift to more positive values as the inhibitor is added into the geothermal fluid. This shows that the inhibitors act anodic. Corrosion inhibition is greatest at concentrations of 1×10^{-3} mol/dm^3 M $C_4H_2O_3$, 1×10^{-2} mol/dm^3 and 1×10^{-3} mol/dm^3 $C_6H_4Na_2O_6S_2$, and 1×10^{-2} and 1×10^{-3} mol/dm^3 $Na_5P_3O_{10}$ (Table 2) solutions.

Corrosion increases with increasing salinity. The conductivity increases because of salts in the geothermal fluid (dissolved oxygen, H^+ ion, Cl^- ion, H_2S, CO_2, NH_3, SO_4^{2-}, HCO_3^-, and CO_3^{2-}) and, as a result, corrosion increases, too. Due to its acidic character, CO_2 in geothermal fluids may influence corrosion directly and indirectly by creating protective layers of $CaCO_3$. The carbonate hardness results from CO_3^{2-} and HCO_3 ions (Ref 32). As carbonate hardness is low, non-carbonate hardness is almost close to total hardness.

Non-carbonate hardness results from the salts of Cl^- and SO_4^{2-} ions. The corrosion rate increases with increasing salt concentration. So that chloride and sulfate deposits increase in pipes in contact with geothermal fluid. Cl^- ions are the most important factor in corrosion, especially in pitting corrosion. According to the oxide film theory, Cl^- ions penetrate through pores or defects of the oxide film than the others ions (e.g., SO_4^{2-}). Or Cl^- may be colloidally disperse the oxide film and increase its permeability. Breakdown of passivity by Cl^- ion occurs locally rather than generally over the passive surface, the preferred sites being determined perhaps by small variations in the passive film structure and thickness. The inhibitors showed surface coverage of approximately 68 and 96%. The surface coverage fraction (θ) of absorbing material can be close to 1. This means the rate of expected reactions on the surface slows down because the surface is almost completely covered.

3.3 The Result of XRD Analysis

XRD analysis of a scale sample (Fig. 3) from the pipe's inner surface shows it to be entirely $CaCO_3$. When $CaCO_3$

precipitates it can form crystals of various polymorphic structures or an amorphous deposit. There are three polymorphic forms of $CaCO_3$ crystals: calcite, aragonite, and vaterite. Their formation depends mainly on the conditions under which the precipitation occurs, mainly the solution temperature. Subsequent transformation, particularly in the case of vaterite, can occur. Each polymorph is easily recognized by the shape of the crystals it forms: cubic for calcite, needle-shaped for aragonite, and spherical for vaterite. Calcite, aragonite, and vaterite have different solubility properties, vaterite being the most and calcite the least soluble phase over a temperature range between 273 and 363 K.

3.4 The Results of IC and ICP-OES Analyses

The results of IC and ICP-OES analysis of geothermal fluids are shown in Table 6.

Geothermal can be categorized under three groups according to its temperature; low (293-343 K), middle (343-423 K), and high (423 K and more) (Ref 33). The temperature of the fluid taken from AF11 well is 383 K. This shows that the geothermal fluid of this well is located in the average geothermal group. All fluid samples include high levels of Ca^{2+} ions, which supports $CaCO_3$ formation. Ca^{2+} concentration in geothermal fluid is related to solubility of $CaCO_3$ (calcite, aragonite), $CaSO_4$ (anhydride, gypsum), CaF_2, and other calcium minerals which are commonly observed in nature.

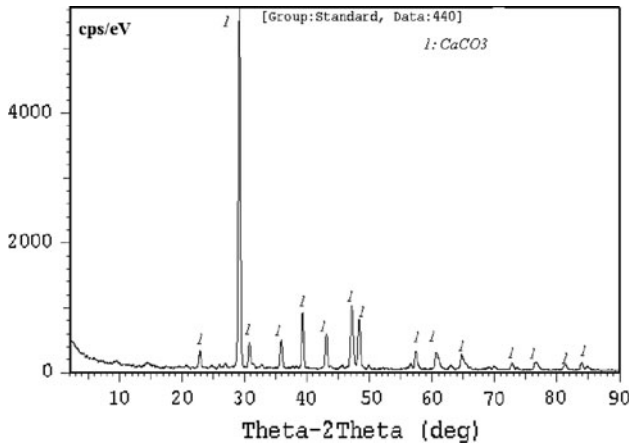

Fig. 3 XRD analysis of scale sample present in the pipe's inner side of geothermal water's exit point (in natural conditions)

In high temperature systems, Ca^{2+} concentration in hot water is generally lower than 50 mg/dm^3 (Ref 34). The Ca^{2+} content of AF11 is 21.8 mg/dm^3. It is 149.9 mg/dm^3 in the collection pool. On reinjection, Ca^{2+} increases to 164.6 mg/dm^3. Na^+/Ca^{2+} ratios can be used as a geothermometer. These values have been calculated from EDX field analyses for st 37 steel are shown in Table 7.

It is accepted that high values of Na^+/Ca^{2+} ratio imply a direct feed from the reservoir (Ref 35). Mg^{2+} concentrations in high temperature (>423 K) geothermal fluid (Ref 33) are between 1×10^{-3} and 1×10^{-1} mg/dm^3. pH values in geothermal water between 6.1 and 7.45. Geothermal water which is high in temperature reduces $CaCO_3$ by the effect of CO_2 via partial pressure effect. Higher concentrations of Ca^{2+} ions (Table 6) show that the source is feed from rock close to the surface or shallow water (Ref 36). In geothermal fluid, the amount of fluorine is generally <10 mg/dm^3. The formation of iron sulfide scale creates serious problems. Iron sulfide is cathodic compared to iron, so it forms galvanic cells which create serious pitting corrosion. The occurrence of all kinds of precipitation in geothermal fluids which include gases like H_2S, O_2, or CO_2 increases the intensity of the probable corrosion problem. Many other studies of scales occurring in steel pipes in geothermal applications show trace amounts of various elements resulting from corrosion of metallic parts of the system (Ref 34). P, Cr, Mn, Ni, and Mo trace elements resulting

Table 7 Calculated Na^+/Ca^{2+} ratios from EDX field analyses (at.%)

	Na^+	Ca^{2+}	Na^+/Ca^{2+} ratios
AF11 for 2 days	6.02	1.52	3.96
AF11 for 9 days	4.73	0.52	9.10
AF11 + first mixed inhibitor for 2 days	2.44	0.64	3.81
AF11 + first mixed inhibitor for 9 days	1.47	…	1.47

Table 6 The results of IC and ICP-OES analyses of geothermal fluids (as mg/dm^3)

The results of IC analyses of geothermal fluids

	Fl^-	Cl^-	NO_2^-	Br^-	NO_3^-	PO_4^{3-}	SO_4^{2-}
AF11	4.71	1810	…	…	…	…	506
Reinjection	4.63	1.850	…	…	…	…	500
Collection pool	4.75	1.842	…	…	…	…	496

The results of ICP-OES analyses of geothermal fluids

	B^{+3}	Ca^{+2}	Fe^{+2}	K^+	Li^+	Mg^{+2}	Mn^{+2}
AF11	9.793	21.8	0.409	138.2	2.808	15.21	0.008
Reinjection	9.449	164.6	0.314	133.1	2.678	15.07	0.029
Collection pool	9.621	149.9	0.4	134.3	2.667	15.03	0.032

… not determined

Table 8 EDX field analyses (wt.%)

	Fe	C	N	O	Na	Si	P	S	Mg	Cl	K	Ca
bare	97.72	2.78	…	…	…	…	…	…	…	…	…	…
AF11 for 2 days	49.91	…	…	31.64	4.84	4.53	…	0.50	0.54	5.34	0.57	2.14
AF11 for 9 days	53.97	0.24	…	30.29	3.72	5.44	…	0.40	0.29	4.52	0.43	0.71
AF11 + first mixed inhibitor solution for 2 days	78.10	3.66	4.02	9.89	1.55	1.12	0.58	0.37	…	…	…	0.71
AF11 + first mixed inhibitor solution for 9 days	79.42	3.17	3.51	10.91	0.92	1.22	0.53	0.32	…	…	…	…

… not determined

from steel corrosion are seen in water taken from geothermal pipelines (Table 8).

The reservoir and well waters of the Omer-Gecek region are predominantly of Na-Cl character for some samples and Na-HCO_3 character for others. The water contains boron in high rate. The geothermal fluid in the Omer-Gecek geothermal region, where the temperatures are between 305 and 365 K, shows variations in the amount of chemical compounds and TDS. Omer-Gecek geothermal fluids have usually the character of Na-Cl-HCO_3, which suggests a probable deep water cycle. The mineral equilibrium is largely controlled by the CO_2 concentration (Ref 35, 37). In the systems whose temperature is high Ca^{2+} concentration dissolved in hot water is usually <50 mg/dm^3. Scale precipitation affects the corrosion of metal. Protection against corrosion is obtained by precipitation of $CaCO_3$ scale, sometimes intentionally. However, scale precipitation often accelerates corrosion. The reason for the low sulfate concentrations determined in the geothermal fluids is quite probably the reduction of bacterial sulfate. Sulfate-reducing bacteria chemically reduce sulfates to sulfides, producing compounds such as hydrogen sulfides (H_2S), or iron sulfide (FeS) in the case of ferrous metals. For each equivalent of hydrogen atoms they consume, one equivalent of Fe^{2+} enters solution to form rust and FeS. The bacteria, therefore, probably eat essentially as depolarizers. The reaction sequence can be outlined as follows:

$$\text{Anodic}\quad 4Fe(s) \rightarrow 4Fe^{2+} + 8e^- \qquad \text{(Eq 4)}$$

$$\text{Katodic}\quad 8H_2O(l) \rightarrow 8H^+ + 8OH^- \qquad \text{(Eq 5)}$$

$$8H^+ + CaSO_4 \rightarrow 4H_2O + CaS + 8e^- \qquad \text{(Eq 6)}$$

$$CaS + 2H_2CO_3 \rightarrow Ca(HCO_3)_2 + H_2S \qquad \text{(Eq 7)}$$

$$\text{Overall reaction}: \quad 4Fe + 8H_2O + CaSO_4 + 2H_2CO_3 \rightarrow 3Fe(OH)_2 + FeS + Ca(HCO_3)_2 \qquad \text{(Eq 8)}$$

Severe damage by sulfate-reducing bacteria has been observed particularly in oil-well casing, buried pipelines, water cooled rolling mills, or pipe from deep water wells (Ref 26).

3.5 The Results of Surface Analyses

St 37 steel was immersed in both the geothermal fluid taken from AF11 well without inhibitor and in the AF11+ first mixed inhibitor solution for 2 and 9 days (at 298 K). Their EDX field analyses are shown in Table 8.

In the point EDX analysis, there are only Fe^{2+}, Fe^{3+} ions on bare surface of st 37 steel (Table 8). When the st 37 steel is examined after immersion in AF11 for 2 days, the atoms found in the surface are O, Na, Mg, Si, S, Cl, K, Ca, and Fe. This shows that this geothermal fluid dissolves many of the constituent elements inside. Oxygen is found in solution in the geothermal fluid, in the form of hydroxides and oxides of iron. The corrosion products of iron are known to be $Fe(OH)_2$, $Fe(OH)_3$, Fe_3O_4, Fe_2O_3, and FeO. The existence of Ca^{2+}, Mg^{2+}, and Si^{2+} on the surface supports scale formation.

When the scale occurs on the surface, the part under the scale becomes anodic. The other parts of surface act as the cathode and the material suffers pitting corrosion. Excess Cl^- ions support pitting corrosion. The oxygen on the surface supports scale formation in the form of $CaCO_3$, $Mg(OH)_2$, and SiO_4. Fe^{2+}, O^{2-}, Mg^{2+}, Ca^{2+}, and S^{2-} were seen to be distributed homogenously across the surface. The fact that Na^+ and Cl^- were more concentrated in certain areas showed that pitting corrosion had started in those areas. According to Table 8; for st 37 steel after immersion in geothermal fluid AF11+ first mixed inhibitor solution for 2 days, the amounts of C and N were rather high and the amount of oxygen is decreased. A protective film develops in the presence of inhibitor. There are many C, N, P peaks in the EDX spectrum, which form a film on the surface and show a cathodic depolarization effect. When the structure of the inhibitor is examined, Na^+ exists in the form of positively charged ions on the outside of both inhibitors, which increases adsorption and protects the surface from aggressive ions like Cl^-. There are Cl^- ions in the solution. There are not Cl^- ions on surface of metal. It may be mentioned that there is competitive adsorption in the inhibitor molecules between Cl^- and Na^+ ions. Na^+ and P come from $Na_5P_3O_{10}$ and S comes from the dibenzene sulfonic salt. $Na_5P_3O_{10}$ reduces surface scale formation. Dibenzene sulfonic alone also shows high inhibition.

After st 37 steel had been immersed in geothermal fluid AF11 for 9 days, the amounts of Na^+ and Cl^- ions decreased compared with the 2 day values (Table 8). There were a lot of O^{2-} and Fe^{2+} ions on the surface, together with iron hydroxides and oxides, which are corrosion products. They can be seen clearly in the metallographic microscope (Fig. 4). XRD analysis are analyzed on powdered scale sample take from inner side pipe output collection pool in natural conditions. XRD showed that there was $CaCO_3$ scale formation on the surface (Fig. 3). Silicon reaches its highest value, at 5.44 mg/dm^3 which shows that there is silicate scale on the surface in natural conditions (Table 8). The concentrations of most other elements vary little between the 2 and 9 day immersion periods. While carbon and nitrogen (with inhibitor geothermal

fluid) increase, silicon, which increases scale formation, has increased. There is no Cl^- ion in immersed AF11+ first mixed inhibitor solution for 2 and 9 days. However, it may pass to geothermal fluid in the form of $FeCl_4^-$ complexes. P, Na, and S, which exist in the inhibitor structure, have held on the surface. The fact that the surface has not been destroyed shows that a film occurs on the surface that controls the corrosion and scale formation. In the point analysis carried out after a 2 day immersion of st 37 iron in AF11, FeO_2^- and FeO occurs on the surface. On the other hand, in the EDX field point analysis carried out after a 9 day immersion of st 37 steel in AF11, a complex of Fe_2O^{2+} structure occurs on the surface. These are effective in protecting the surface against corrosion and scale formation.

The SEM and metallographic photomicrographs are shown in Fig. 4, 5, and 6.

Figures 4, 5, and 6 show that there were polishing faults in all microphotographs. The surface images from bare st 37, AF11 + 2 days with inhibitor and AF11 + 9 days with inhibitor (Fig. 4, 5, and 6a, c, e) are similar to one another. The photomicrographs with inhibitor (Fig. 4, 5, and 6a, c, e) are better than the bare surface, which shows that inhibitors form a thin film on the surface and decrease corrosion and scale formation. The surfaces without inhibitor are rougher and they

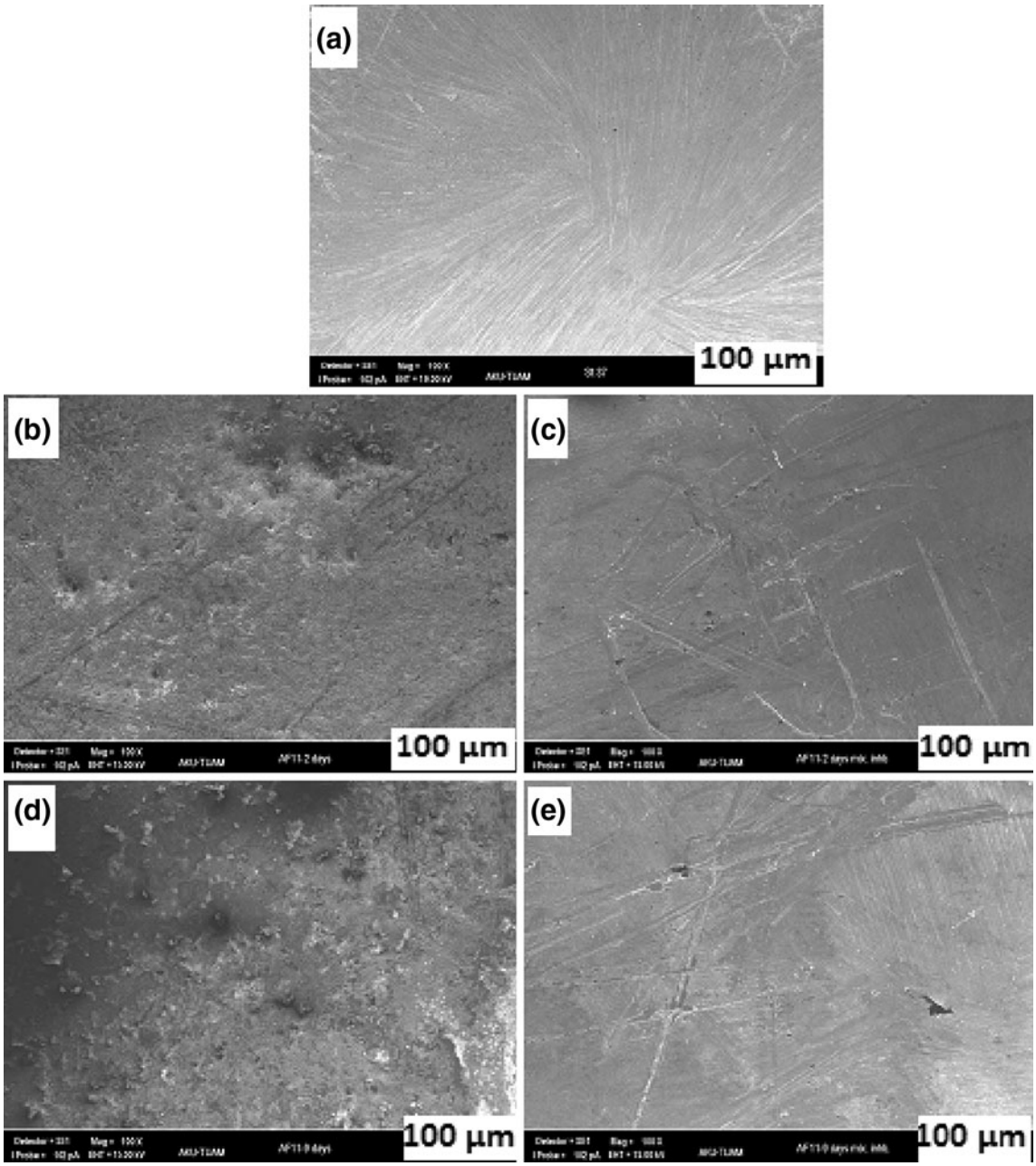

Fig. 4 The SEM microphotographs of st 37 steel (a) bare st 37 steel, (b) AF11 + 2 days, (c) AF11 + 2 days first mixed inhibitor solution, (d) AF11 + 9 days, and (e) AF11 + 9 days first mixed inhibitor solution (first mixed inh: 1×10^{-3} mol/dm^3 $C_4H_2O_3$ + 1×10^{-2} mol/dm^3 $C_6H_4Na_2C_6S_2$ + 1×10^{-3} mol/dm^3 $Na_5P_3O_{10}$)

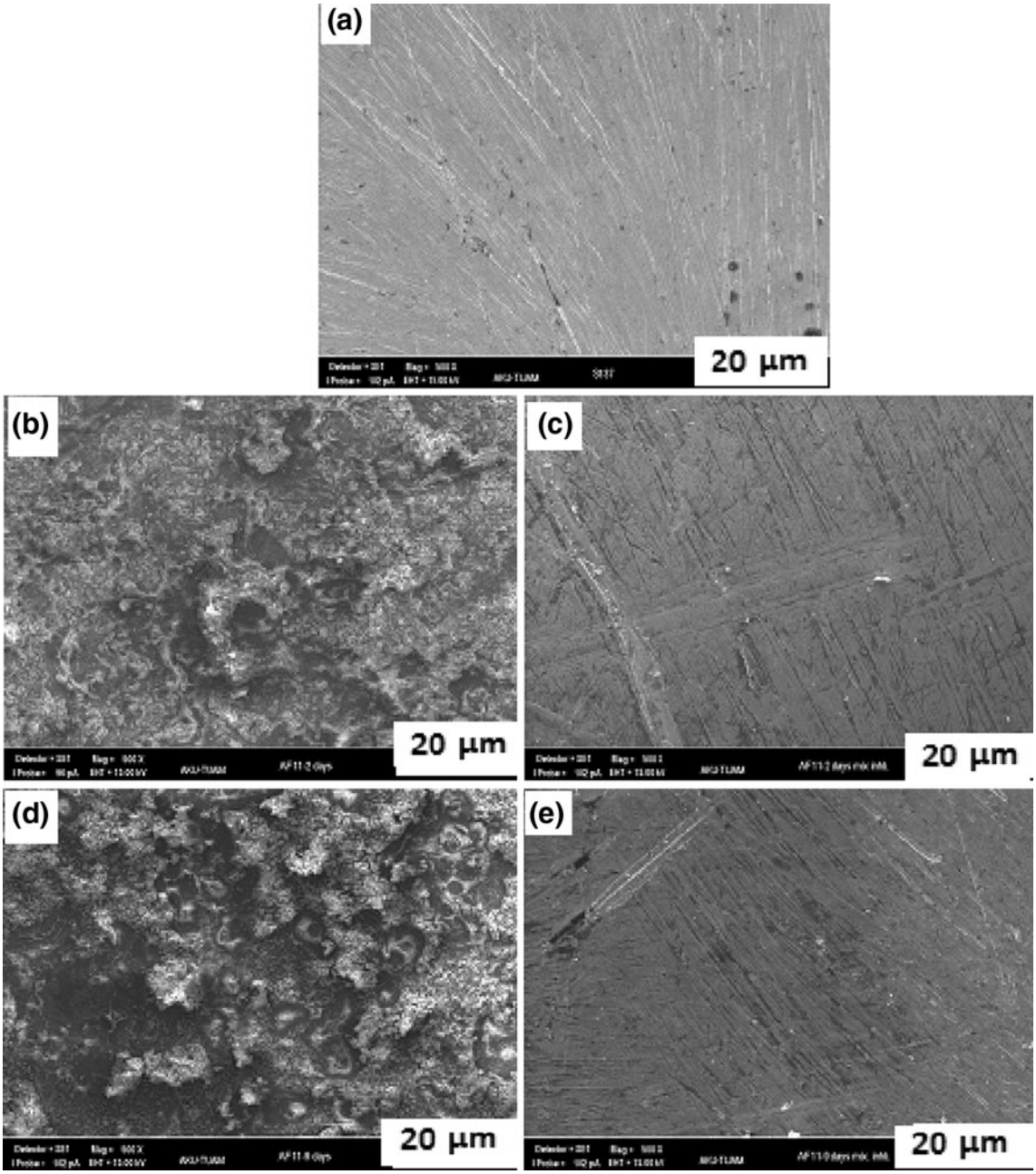

Fig. 5 The SEM microphotographs of st 37 steel (a) bare st 37 steel, (b) AF11 + 2 days, (c) AF11 + 2 days first mixed inhibitor solution, (d) AF11 + 9 days, and (e) AF11 + 9 days first mixed inhibitor solution (first mixed inh: 1×10^{-3} mol/dm^3 $C_4H_2O_3$ + 1×10^{-2} mol/dm^3 $C_6H_4Na_2C_6S_2$ + 1×10^{-3} mol/dm^3 $Na_5P_3O_{10}$)

are not homogeneous (Fig. 4, 5, and 6b, d). The surfaces are exposed to corrosion. When EDXs of the samples above are examined (Table 8), there are usually FeO^{2-} ions on the surface without inhibitor and Fe_2O^{+} ion on the surface with inhibitor. As there is an excess of charge in FeO^{2-}, it accelerates the corrosion. Fe_2O^{+} decreases corrosion and scale formation by holding on the surface. Iron forms hydroxides first and then transforms into oxides, as it corrodes. The iron corrodes slightly and the corrosion products produce a protective structure on the surface by uniting with inhibitors.

The basis of these comments is seen clearly in the enlarged SEM microphotographs (Fig. 6). When Fig. 6(b) is compared with d, the surface has corroded little in 2 days, but more in 9 days. As the surface is little covered with iron oxides and hydroxides in 9 days, Fig. 6(b) is not very different from Fig. 6(d). The results with inhibitor are very similar to each other.

4. Conclusions

- 96% inhibition is seen in AF11 + 1×10^{-3} mol/dm^3 $C_4H_2O_3$ + 1×10^{-2} mol/dm^3 $C_6H_4Na_2O_6S_2$ + 1×10 3 mol/dm^3 $Na_5P_3O_{10}$, the first mixed inhibitor solution. 90% inhibition is seen in AF11 + 1×10^{-2} mol/dm^3

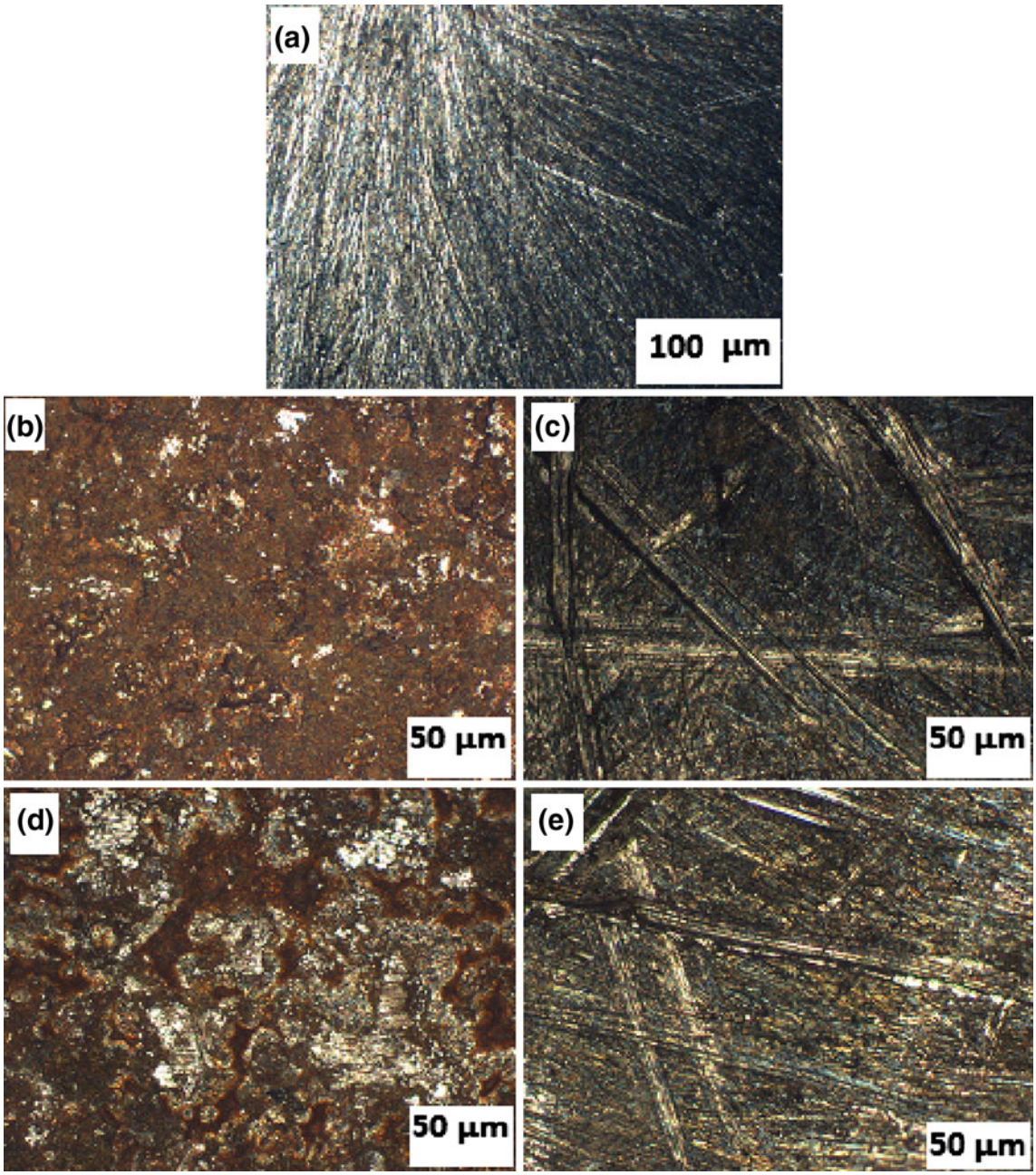

Fig. 6 The metal microscopy microphotographs of st 37 steel (a) bare st 37 steel, (b) AF11 + 2 days, (c) AF11 + 2 days first mixed inhibitor solution, (d) AF11 + 9 days, and (e) AF11 + 9 days first mixed inhibitor solution (first mixed inh:1×10^{-3} mol/dm^3 $C_4H_2O_3$ + 1×10^{-2} mol/dm^3 $C_6H_4Na_2C_6S_2$ + 1×10^{-3} mol/dm^3 $Na_5P_3O_{10}$)

$C_6H_4Na_2O_6S_2$ + 1×10^{-3} mol/dm^3 M $Na_5P_3O_{10}$, the second mixture inhibitor solution.

- 90% inhibition is also seen in the AF11 + 1×10^{-2} mol/dm^3 $C_6H_4Na_2O_6S_2$ solution. $C_6H_4Na_2O_6S_2$ can therefore be used on its own.
- If pH ≥ 8 as a result of adding inhibitor, corrosion will decrease.
- The tested inhibitors act as anodic inhibitors.
- XRD analysis shows that there is $CaCO_3$ aragonite scaling in the system.
- As TDS, salinity, conductivity decrease, inhibition increases. Increasing TDS, alkalinity, and hardness all promote scale formation.
- The microphotographs of SEM and metal microscope show that the tested inhibitors form a protective film on the surface.
- The EDX results show the presence of the Fe_2O^+ ion on the surface of st 37 steel which has been immersed in the solution with inhibitor for 2 and 9 days. FeO^{2-} ion occurs in the medium without inhibitor. FeO^{2-} accelerates the corrosion because of its excess of charge. Fe_2O^+ decreases corrosion and scale formation by adsorbing onto the surface.
- IC and ICP-OES analyses show that the geothermal fluid form is of Na-Cl-HCO_3 type, while the high Na^+/Ca^{2+} ratios show that the fluid is directly from the reservoir. The very

high levels of Ca^{2+} revealed by the IC and ICP-OES analyses support scale formation. High sulfate concentrations in the water are caused by reduction of bacterial sulfate.

Acknowledgment

The authors thank the personnel of AFJET for their help and the sharing of information.

References

1. P.J. Lienau and K. Rafferty, Piping Geo-Fluids, *Bull. Geo-Heat Center*, 1986, **9**, p 5–8
2. R. Corsi, Scaling and Corrosion in Geothermal Equipment; Problems and Preventive Measures, *Geothermics*, 1986, **15**(5-6), p 839–856
3. P. Ungemach and R. Turon, Injection en fond de puits d'agents inhibiteurs de corrosion/incrustation, *Geothermics Actualities*, 1988, **5**, p 31–40
4. B. Gautier, O. Goyeneche, and J. Duvivier, La prévention de la corrosion en géothermie. Etat des travaux de recherches en France (Corrosion prevention in geothermal resource exploitation), *Reseaux et Chaleur*, 1990, **5**, p 57–63 (in French)
5. S. Pieri, F. Sabatelli, and B. Tarquni, Field Testing Results of Downhole Scale Inhibitor Injection, *Geothermics*, 1989, **18**, p 249–257
6. M. Parlaktuna and E. Okandan, The Use of Chemical Inhibitors for Prevention of Calcium Carbonate Scaling, *Geothermics*, 1989, **18**, p 214–248
7. G. Batis, N. Kouloumbi, and K. Kotsakou, Corrosion and Protection of Carbon Steel in Low Enthalpy Geothermal Fluids. The Case of Sousaki in Greece, *Geothermics*, 1997, **26**(1), p 65–82
8. V. Soylemezoglu and R. Harper, Oxygen Ingress into Geothermal Steam and Its Effect on Corrosion of Low Carbon Steel at Broadlands; New Zealand, *Geothermics*, 1982, **11**(1), p 31–42
9. A.G. Xyla, J. Mikroyannidis, and P.G. Koutsoukos, The Inhibition of Calcium Carbonate Precipitation in Aqueous Media by Organophosphorus Compounds, *J. Colloid Interface Sci.*, 1992, **153**(2), p 537–551
10. D.L. Gallup, The Use of Reducing Agents for Control of Ferric Silicate Scale Deposition, *Geothermics*, 1993, **22**(1), p 39–48
11. D.L. Gallup, Aluminum Silicate Scale Formation and Inhibition: Scale Characterization and Laboratory Experiments, *Geothermics*, 1997, **26**(4), p 483–499
12. A.P. Morizot and A. Neville, Insights into Electrodeposition of an Inhibitor Film and Its Inhibitive Effects on Calcium Carbonate Deposition, *J. Colloid Interface Sci.*, 2002, **245**, p 40–49
13. D.L. Gallup and E. Barcelon, Investigations of Organic Inhibitors for Silica Scale Control from Geothermal Brines-II, *Geothermics*, 2005, **34**, p 756–771
14. S. Richter, L.R. Hilbert, and R.I. Thorarinsdottir, On-Line Corrosion Monitoring in Geothermal District Heating Systems. I. General Corrosion Rates, *Corros. Sci.*, 2006, **48**(7), p 1770–1778
15. J. Banas, U. Lelek-Borkowska, B. Mazurkiewic, and W. Solarski, Effect of CO_2 and H_2S on the Composition and Stability of Passive Film on Iron Alloys in Geothermal Water, *Electrochim. Acta*, 2007, **52**, p 5704–5714
16. TS 266, *The Physical and Chemical Properties of Drinking Water*, Turkish Standart, 1984 (in Turkish)
17. M. Erbil, *Corrosion Inhibitors and the Determine of Inhibitor Efficiency*, Segem Issues, Ankara, Turkey, 1984,146 pp (in Turkish)
18. S. Uneri, *Korozyon ve Önlenmesi* (Corrosion and Protection), The Corrosion Association Publisher, Ankara, Turkey, 1998, 413 p (in Turkish)
19. J.S. Gill and M.A. Yorke, *Calcium Carbonate Control in Highly Supersaturated Aqueous Environment, CORROSION/94, Paper 195*, NACE, Houston, TX, 1994
20. J.D. Sallis, W. Juckes, and M.E. *Anderson, Mineral Scale Formation and Inhibition*, Z. Amjad, Ed., Plenum, New York, 1995, p 87
21. M.C. Van Der Leeden and G.M. Van Rosmalen, Adsorption Behavior of Polyelectrolytes on Barium Sulfate Crystals, *J. Colloid Interface Sci.*, 1995, **171**(1), p 142–149
22. W.J. Benton, I.R. Collins, I.M. Grimsey, G.M. Parkinson, and S.A. Rodger, Nucleation, Growth and Inhibition of Barium Sulfate-Controlled Modification with Organic and Inorganic Additives, *Faraday Discuss.*, 1993, **95**, p 281–297
23. S. Patel and A.J. Nicol, Developing a Cooling Water Inhibitor with Multifunctional Deposit Control Properties, *Mater Perform.*, 1996, **35**(6), p 41–47
24. G.E. Geiger, Improve Corrosion and Deposition Control in Alkaline Cooling Water Systems, *Hydrocarbon Process.*, 1996, **75**(1), p 93–98
25. E. Mueller, C.S. Sikes, and B.J. Little, Peptide Interactions with Steel Surfaces: Inhibition of Corrosion and Calcium Carbonate Precipitation, *Corrosion*, 1993, **49**(10), p 829–835
26. H.H. Uhlig, *Corrosion and Corrosion Control*, 2nd ed., Wiley, New York, 1985, 419 pp
27. G. Kreysa and M. Schütze, eds., *Corrosion Handbook*, 2nd ed., Wiley, New York, 2009
28. M. Pourbaix, Thermodynamics and Corrosion, *Corros. Sci.*, 1990, **30**, p 963–988
29. J. Featherstone, S. Butler, and E. Bonham, Comparison of Crystallizer Reactor-Clarifer and pH Modification Process Technologies Used at the Salton Sea Geothermal Fluid, P*roceedings of World Geothermal Congress*, Vol. 4, Florence, 1995, p 2391–2396
30. D. Hoyer, K. Kitz, and D. Gallup, Salton Sea Unit 2—Innovations and Successes, *Geotherm. Resour. Council Trans.*, 1991, **15**, p 355–361
31. A. Manceau, Ph. Ildephonse, J.L. Hazemann, A.M. Flank, and D. Gallup, Crystal Chemistry of Hydrous Iron Silicate Scale Deposits at the Salton Sea Geothermal Field, *Clays Clay Mineral.*, 1995, **43**, p 304–317
32. A.E. Al-Rawajfeh, H. Gladeb, and J. Ulrich, Scaling in Multiple-Effect Distillers: The Role of CO_2 Release, *Desalination*, 2005, **182**, p 209–219
33. V. Eroğlu, The Use and Fountain of Thermal, Mineral Water in Turkey, *Thermal and Mineral Water Lecture*, A.E. Türker and A. Yildiz, Ed., Afyonkarahisar Kocatepe University, Sozkesen Publisher, Afyonkarahisar, Turkey, 24–25 April 2008, p 3–11 (in Turkish)
34. A. Şahmurova, E. Hepsağ, and A. Özkan, Trace Element Concentrations in Groundwaters in Azerbaıjan and Assessment of Fluoride Concentration, *Trakya Univ. J. Sci.*, 2005, **6**(2), p 57–63
35. H. Mutlu, Ph.D. Thesis, METU, Graduate School of Natural and Applied Sciences, Ankara, 1996
36. B. Akan and S. Suer, The Investigation of Geothermal Fields in Afyon, *Thermal and Mineral Water Lecture*, A.E. Türker and A. Yildiz, Ed., Afyonkarahisar Kocatepe University, Sozkesen Publisher, Afyonkarahisar, Turkey, 24-25 April 2008, p 97–105 (in Turkish)
37. H. Mutlu, The Chemical Properties of Omer-Gecek (Afyon) Geothermal Water, *Thermal and Mineral Water Lecture*, A.E. Türker and A. Yildiz, Ed., Afyonkarahisar Kocatepe University, Sozkesen Publisher, Afyonkarahisar, Turkey, 24-25 April 2008, p 215 (in Turkish)